Numerical prediction of off-design performance for a Power-to-Gas system coupled with renewables

(Article begins on next page)

06 October 2024

Numerical prediction of off-design performance for a Power-to-Gas system coupled with renewables

M. A. Ancona, M. Bianchi, L. Branchini, F. Catena[*]**, A. De Pascale, F. Melino, A. Peretto**

Alma Mater Studiorum, Università di Bologna - DIN, viale del Risorgimento 2, Bologna, 40136, Italy

*corresponding author:

Abstract

In this study, the off-design performance of a Power-to-Gas process are predicted by means of a developed calculation model, implemented in commercial tool environments. With the aim to evaluate the behaviour of the several components in off-design conditions, specific calculation models have been integrated in the whole system model. Then, starting from a real wind production profile, four configurations of the Power-to-Gas system have been analysed, evaluating the annual operating time of the integrated Power-to-Gas/wind systems. In addition, in order to assess the cost effectiveness of the technology, a preliminary economic analysis has been performed. The results highlight that the most performant configuration is the one at ambient pressure, with the co-electrolyzer and the high temperature methanation section operating at the same temperature, showing a methane production of 184 ton/year and an overall efficiency of about 75 %. At the current technology readiness level, the economic competitiveness of the process is strongly affected by the synthetic natural gas sell price.

Keywords: Power-to-Gas; co-electrolysis; methanation; storage system; off-design performance; renewables.

1. Introduction

One of the main targets in many Countries is the decarbonization of the energy sector, as also defined in the European Roadmap 2050 [1]. In order to achieve this goal, a possible solution is to increase the penetration of Renewable Energy Sources (RES) into the electrical system. However, RES such as wind and solar supply electrical power in an intermittent way. This volatility results in issues related to the management of local and regional electric networks, due to the several hours and even days of electricity surplus and deficit. Indeed, as reported by Karimi et al. [2], despite its promising success, photovoltaic

---

[*] Corresponding author

28   (PV) penetration presents various issues, such as voltage fluctuation, voltage rise and voltage balance, and its impact on the

29   distribution system has to address for seamless integration in the power system. Moreover, Eltawil et al. [3] have evaluated the

30   operation of grid-connected PV generators, demonstrating that control problems can be registered as a consequence of the

31   variable power generation. Similar problems arise in case of wind generators, which are affected by a short-term non-

32   programmable and intermittent power production and also by a long-term variability [4].

33   As the share of these sources in power generation increases, long term and even seasonal storage capacities are required to

34   ensure a reliable energy supply. In this context, the needed flexibility to balance the stochastic energy production and then to

35   make easier the RES integration in the electric network can be offered by the emerging technology of Power-to-Gas (P2G) [5],

36   i.e. the process of converting the surplus of renewable energy into a gas fuel. As reported by Yang et al. [6], the P2G energy

37   conversion method can provide an effective solution to the energy dilemma; indeed, this technology can be seen as a flexible

38   energy-use mechanism to absorb redundant renewable energy and to mitigate the natural gas supply shortage for power plants

39   in the meantime. Sayedin et al. [7] claim that although most of the renewable energy technologies are well known, the

40   integration of these technologies has still some issues; the mismatch between the output specification of photovoltaic modules

41   and electrolyzers load at different irradiance conditions indicates the importance of the optimal matching of the photovoltaic

42   and electrolyzers. For this reason, the Author's investigation is based on the evaluation of the behaviour of an innovative P2G

43   process at various loading conditions, considering the variability of the electric energy supply. Indeed, the P2G process can be

44   considered a viable flexible technology [8]; as presented by Kupecki et al. [9], the solution of the grid imbalances can be

45   represented by an electrolyzer, which mitigates the problem by coupling the electric and gas grids. Petipas et al. [10] show that

46   with the addition of control strategies, electrolyzers should operate across a wider load range, even below 60 % of the design

47   load. As a consequence, the loading power of a P2G system can follow the fluctuating demand and then balance the

48   intermittent RES production [11]. According to Frank et al. [12], reversible solid oxide cells represent a promising approach in

49   order to guarantee a constant power supply. With this purpose, the renewable energy that might be wasted (peak production)

50   can be exploited to produce useful fuel gases. Following this way, several P2G pilot plants have been realized worldwide, as

51   shown by Gahleitner [13].

52   The Solid Oxide Electrolyte Cell (SOEC) technology is currently on research and development level and there are not many

53   publications related to the modelling of its operations, especially in off-design conditions (i.e. when the input power differs

54   from the design value). One of the few studies about the off-design characteristics of a SOEC is that presented by Motylinski et

55   al [14], in which a SOEC operated in electrolysis mode has been modelled and analysed; the used methodology derives from a

56   solution used to predict the performance of fuel cell power units with solid oxide technology, both in steady-state [15] and in

57   transient operations [16]. Furthermore, as reported by Safari et al. [17], the Synthetic Natural Gas (SNG) generated by the P2G

58 plant can be fed into the existing gas grid and marketed as an emission-free option for SNG-fuelled users; since the capacity

59 for SNG is high around the world and the methanation process captures CO_2, the SNG production can be the most promising

60 P2G technology.

61 In this framework, the innovative step of the Authors' study is the numerical prediction of off-design performance for a P2G

62 process including a SOEC operated in co-electrolysis [18] mode. Indeed, the aim of this study mainly stands in the

63 development of a calculation model for the off-design operations of the P2G process, focusing on a particular and innovative

64 P2G system based on a high temperature co-electrolyzer (simultaneous electrolysis of H_2O and CO_2) of SOEC technology

65 coupled with an advanced experimental methanator, which allows to operate at relatively high temperatures.

66 This work is a prosecution of Author's previous study [19], whose novelty stood in the development and analysis of the P2G

67 system, considering the possibility to thermally integrate the electrolysis with the methanation process, as a first step towards a

68 physical integration between the two components. In this previous study, the analysis has been carried-out in design condition,

69 considering all the sub-sections working at their set-points of operating temperature and pressure. In order to evaluate the

70 behaviour of the several components in off-design conditions a numerical code has been developed in the study here reported.

71 In more detail, the code has been developed in commercial tool environments and it is able to predict the operating point shift

72 of the several components during the off-design operations. The analysed key parameters are the operating temperature and

73 pressure. The pressurization of the system has been investigated since it can [20]:

74 - increase the SOEC power density;

75 - improve the produced SNG quality;

76 - reduce the size of the auxiliary components.

77 Furthermore, different temperature settings have been evaluated in order to explore possible thermal synergies among the sub-

78 sections; the thermal synergy can be achieved operating both the co-electrolyzer and the methanation section within relatively

79 high temperature ranges (in particular, the co-electrolysis operation at intermediate temperature has been demonstrated in a

80 work by Lo Faro et al. [21]). In addition, in order to predict co-electrolysis behaviour under several conditions, a specific

81 calculation sub-model has been integrated in the whole system model. Then, in order to evaluate the off-design performance of

82 the P2G process under different operating conditions, four system variants have been analysed, starting from a real wind

83 production profile and evaluating the annual operating time of the integrated P2G-wind systems.

84 In particular, in **Section 2** of the paper the studied P2G system is introduced and the analysed configurations are presented. In

85 **Section 3**, the P2G numerical model for off-design operations is described. In **Section 4** and in **Section 5**, the analysis of the

86 P2G system coupled with a wind generator and a preliminary economic analysis are carried-out. Finally, the results of the

87 performed analyses are provided and discussed in **Section 6**.

2. The Power-to-Gas system: description and analysed configurations

As previously mentioned, the considered P2G process refers to a previous study of the Authors [19], where this innovative P2G system has been proposed. In particular, the innovative feature of the P2G system is the coupling of a high temperature co-electrolyzer (600 - 850 °C) with an experimental advanced methanation reactor, consisting in a fixed-bed reactor with a new formulation of structured catalyst, which allows to operate at relatively high temperatures (450 - 600 °C).

Fig. 1 shows a simplified scheme of the P2G system in study. Briefly, the system is characterized by water and carbon dioxide as main material input streams, while the energy input consists in electric power, from NP-RES (Non-Programmable Renewable Energy Sources), and thermal power, from an external heat source. The main output of the system is a SNG stream, to be introduced into the natural gas (NG) network. The P2G system includes also a sweep-air inlet stream shown in figure, for the SOEC anodic-side products removal (not shown in figure for sake of simplicity), and a tail-end output water stream, separated from the generated SNG.
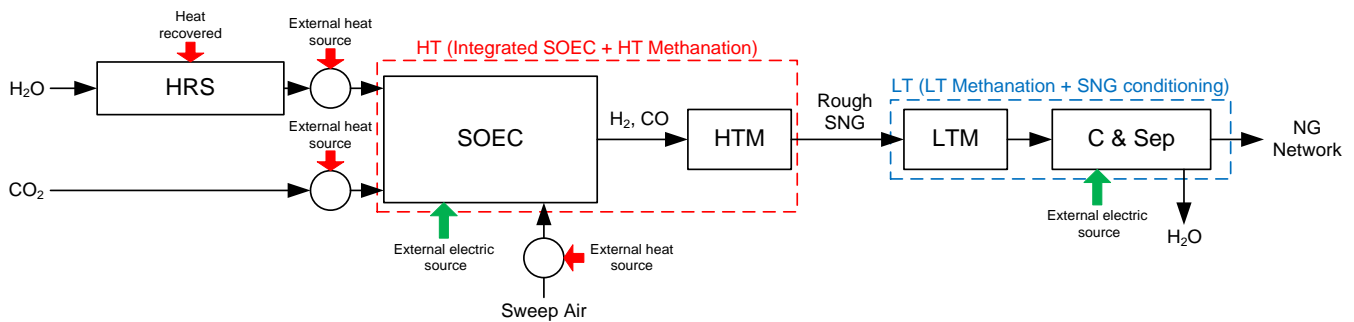
Fig. 1. Simplified block diagram of the P2G system [19].

In more detail, the system is composed by three major sections: a reactants pre-heating section including a HRS (Heat Recovery Section) for the P2G internal heat recovering (used for the inlet water partial preheating, as shown in **Fig. 1**), a high-temperature (HT) section (highlighted in red in **Fig. 1**) and a downstream low-temperature (LT) section (in blue in figure). In particular, the HT section includes the following components:

- a high temperature co-electrolyzer (SOEC in figure), where H_2O and CO_2 are converted into hydrogen and carbon oxide as main species, by means of the electric power input to the P2G storage system;
- a high temperature methanation (HTM) sub-section, where the methanation reactions occur and the reactants are converted into a rough SNG. This sub-section has been modelled on the basis of an experimental structured catalyst.

4

112　The downstream LT section has been introduced in order to improve the quality of the rough SNG produced by the HTM. In

113　particular, the LT section is composed by:

114　　-　a low temperature methanation (LTM) sub-section, based on conventional catalytic methanation technology;

115　　-　an additional SNG processing section, where the SNG is mainly compressed, cooled and separated from residual

116　　　water, before the introduction into the NG distribution network.

117　Regarding the operating temperature, the pressure levels and the heat recovery section arrangement, all of these design settings

118　have been the subject of an in-depth comparative analysis among several configurations reported in [19].

119

120　**2.1 Power-to-Gas system configurations**

121　In order to evaluate the off-design performance of the P2G system under different operating conditions, four configurations

122　have been considered in this study. The key analyzed parameters are the operating pressure and the operating temperature of

123　the several sub-sections of the P2G system; in particular, the pressurization of the P2G system has been investigated since it

124　can significantly increase the SOEC power density, improve the produced SNG quality and reduce the size of the auxiliary

125　components; furthermore, different temperature settings have been evaluated, in order to explore possible thermal synergies

126　among the sub-sections. The choice of the SOEC (and then of the downstream sub-sections) pressure level has generated two

127　different layouts of the P2G system. The first one (**Fig. 2**) is a P2G system with the SOEC and the methanation sections (HTM

128　and LTM) at ambient pressure and with a tail end pressurization, before the introduction into the NG network. The final SNG

129　storage pressure has been set equal to 60 bar, consistent with a high-pressure NG pipeline.

130　The second one (**Fig. 3**) is a P2G system with a pressurized SOEC. Thus, in this system, the HTM and the LTM sections

131　operate at the same pressure of the SOEC; also in this case, at the end of the process the produced SNG is pressurized up to the

132　same final storage pressure (60 bar). As shown in **Fig. 3**, the pressurized layout requires at the inlet a pump for the inlet water

133　stream and a compressor for the inlet carbon dioxide stream. Moreover, the pressurization of the Sweep Air stream has also

134　been considered.

135　Regarding the pressurized layout, for the SOEC (and then for the downstream sub-sections) an operating pressure equal to 8

136　bar has been chosen; this value is in line with the current state-of-the-art of pressurized SOEC technology (even if higher

137　values are also expected in the future – see the HELMETH project [22]) and it corresponds to the experimental data provided

138　in the study by Mehran et al. [23] on a prototypal co-electrolyzer SOEC.

139　Then, for both layouts, two different temperature settings have been considered. Indeed, the studied configurations can be

140　summed up in:

141　- Ambient 1: P2G system at ambient pressure, with the SOEC at 850 °C, the HTM at 450 °C and the LTM at 200 °C;

5

142   - Ambient 2: P2G system at ambient pressure, with the SOEC at 600 °C, the HTM at 600 °C and the LTM at 200 °C;

143   - Pressurized 1: pressurized P2G system, with the SOEC at 850 °C, the HTM at 450 °C and the LTM at 200 °C;

144   - Pressurized 2: pressurized P2G system, with the SOEC at 600 °C, the HTM at 600 °C and the LTM at 200 °C.

145   In the configurations Ambient 1 and Pressurized 1, the SOEC operating temperature has been set equal to 850 °C, in line with

146   high performance SOEC operating conditions, in accordance to the available studies on high temperature SOEC [24]. The

147   HTM operating temperature has been set equal to 450 °C, in order to exploit the HTM highest conversion rate value, according

148   to [19]. The LTM operating temperature has been set after a parametric study of its effect, considering the typical temperature

149   range of operation of this technology [25]. On the other hand, in configurations Ambient 2 and Pressurized 2, in order to

150   explore possible thermal synergies among the sub-sections, different temperature levels have been investigated in the Authors'

151   previous study [19]; in particular, the thermal synergy can be achieved operating both the co-electrolyzer and the methanation

152   section within relatively high temperature ranges (the co-electrolysis operation at intermediate temperature has been

153   demonstrated in a work by Lo Faro et al. [21]).
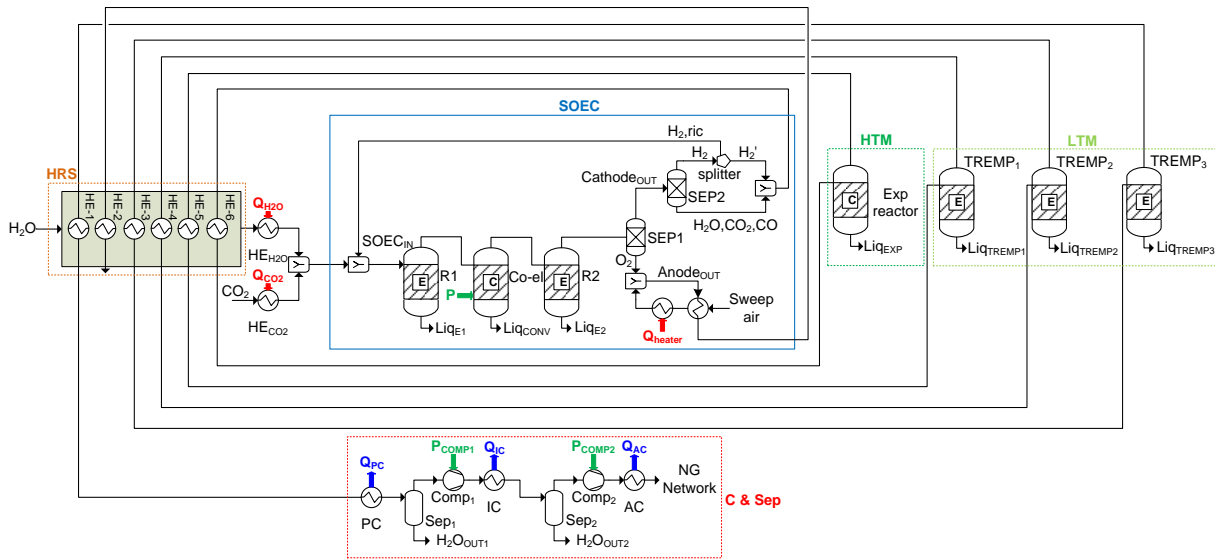
154

155   **Fig. 2**. Layout of the P2G system at ambient pressure.
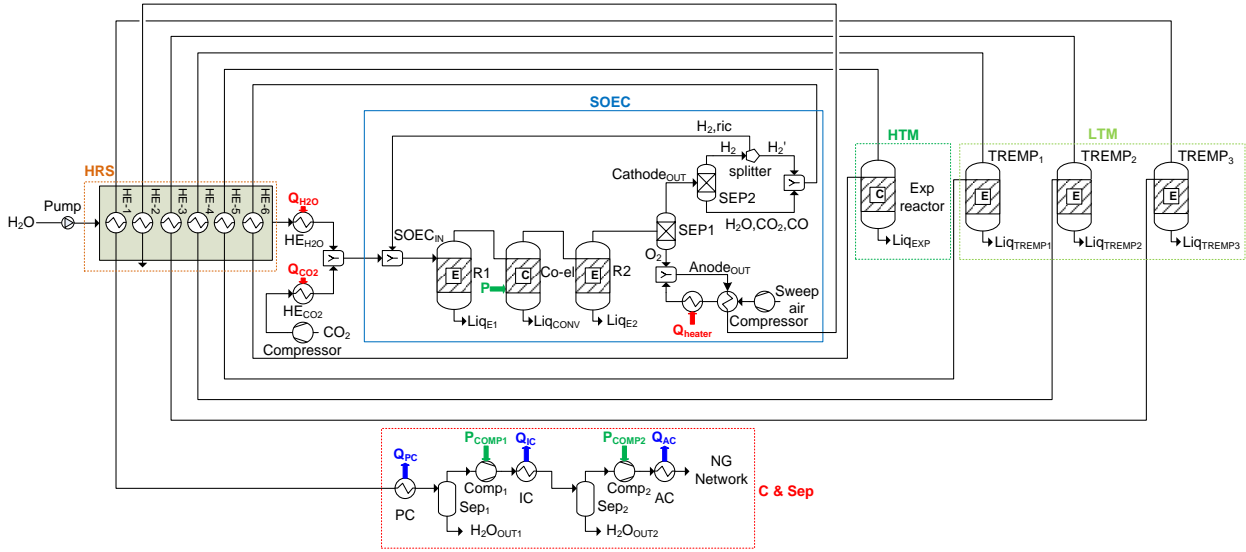
Fig. 3. Layout of the pressurized P2G system.

3. The Power-to-Gas system numerical model

The P2G system thermodynamic model has been developed in ASPEN Hysys^{TM} environment [26], a commercial tool for numerical lumped-parameter modelling of complex energy systems. Standard units from ASPEN Hysys^{TM} library have been employed to model common components, like separators, heat exchangers, pumps and compressors, while specific sub-models have been implemented for the key components of the P2G system. In particular, the thermodynamic model includes:

- a preheating HRS, made by several heat exchanging segments;
- three different reactors for the SOEC, to simulate the electrolytic reactions, the reverse water-gas shift reaction and the methane formation reaction:

$$H_2O \rightarrow H_2 + \frac{1}{2}O_2 \tag{1}$$

$$CO_2 \rightarrow CO + \frac{1}{2}O_2 \tag{2}$$

$$CO_2 + H_2 \leftrightarrow CO + H_2O \tag{3}$$

$$CO + 3H_2 \leftrightarrow CH_4 + H_2O \tag{4}$$

- a conversion reactor for the HTM section;
- a multi-step equilibrium reactor for the LTM section;
- a two-step intercooled final compression, with water separation.

The reactions occurring in the SOEC are mainly influenced by the operating temperature and pressure; in addition, also the mass stream at the inlet of the reactors and the chemical composition of the stream can condition the SOEC behaviour. More details on the thermochemical model, on the reactors arrangements and on the chemical settings, can be found in the previous

7

177 study of the Authors [19], where a parametric design analysis of the P2G system has been carried out, taking into account an
178 electric power supply design point for the SOEC set at 1 MW. Furthermore, in the Authors' study [19], the sensitivity analysis
179 of the ASPEN Hysys^{TM} model on boundary conditions and inlet power condition has been performed.

180 The main set point parameters in design conditions implemented in the P2G system are summarized in **Table 1**. In particular,
181 the conversion rate target of electrolysis reactions is assumed equal or higher than the 80 % in [27]: in this study, a
182 conservative value equal to the 80 % is set. Furthermore, the O_2 molar fraction in the anode outlet is set at 0.5, as
183 recommended in [28]. Finally, in order to allow the introduction of the produced SNG into the NG network, the pressure at the
184 outlet of the systems has been set on the basis of typical values for high pressure lines of the Italian natural gas network [29].

185

186   **Table 1**. Main set point parameters of the P2G system in design conditions for the analysed cases.

Parameter	Ambient 1	Ambient 2	Pressurized 1	Pressurized 2
P2G inlet reactants temperature [°C]	25	25	25	25
P2G inlet reactants pressure [bar]	1	1	1	1
SOEC input electric power [MW]	1	1	1	1
SOEC operating temperature [°C]	850	600	850	600
SOEC operating pressure [bar]	1	1	8	8
SOEC inlet H_2O fraction [% vol.]	80	80	80	80
SOEC inlet CO_2 fraction [% vol.]	20	20	20	20
H_2O electrolysis reaction Conversion Rate [%]	80	80	80	80
CO_2 electrolysis reaction Conversion Rate [%]	80	80	80	80
O_2 molar fraction in the anode stream [-]	0.5	0.5	0.5	0.5
HTM operating temperature [°C]	450	600	450	600
HTM operating pressure [bar]	1	1	8	8
LTM operating temperature [°C]	200	200	200	200
LTM operating pressure [bar]	1	1	8	8
NG distribution network pressure [bar]	60	60	60	60

187

188 As previously mentioned, the aim of this study is the performance prediction of the P2G system both in design and off-design
189 conditions; in particular, the system operates in off-design when the input electric power differs from the design value. In order to
190 take into account the off-design operations, the thermodynamic model developed in ASPEN Hysys^{TM} has been integrated with a

191 specific calculation sub-model for the SOEC, developed in MATLAB^{TM} environment [30], as shown in **Fig. 4**. The carried-out

192 analysis is of quasi-static type; this assumption implies that the considered system has a time-dependent response, but the

193 inertia effects have been neglected. As a consequence, the proposed model does not consider process dynamics. However,

194 since process dynamics (accumulation of mass and energy in the several components of the plant) can play an important role in

195 the estimation of the system performance, this aspect will be considered in future studies.

196

Fig. 4. Simplified block diagram of the numerical procedure for design and off-design analysis of the P2G system.

200 In more detail, the calculation procedure starts with the P2G system layout definition and the thermodynamic design analysis,

201 performed within the ASPEN Hysys^{TM} environment, based on the set point design power input and on the basis of the other system

202 boundary conditions of **Table 1**. This calculation provides as output all the internal and outlet stream flows and enthalpy values,

203 corresponding to the reference inlet power condition. Then, off-design calculation of the same system performance under different

204 electric power inputs can be performed, by interrogating a specific SOEC sub-model (MATLAB^{TM} sub-routine); the SOEC sub-

9

191 specific calculation sub-model for the SOEC, developed in MATLAB[TM] environment [30], as shown in **Fig. 4**. The carried-out

192 analysis is of quasi-static type; this assumption implies that the considered system has a time-dependent response, but the

193 inertia effects have been neglected. As a consequence, the proposed model does not consider process dynamics. However,

194 since process dynamics (accumulation of mass and energy in the several components of the plant) can play an important role in

195 the estimation of the system performance, this aspect will be considered in future studies.

196

Fig. 4. Simplified block diagram of the numerical procedure for design and off-design analysis of the P2G system.

200 In more detail, the calculation procedure starts with the P2G system layout definition and the thermodynamic design analysis,

201 performed within the ASPEN Hysys[TM] environment, based on the set point design power input and on the basis of the other system

202 boundary conditions of **Table 1**. This calculation provides as output all the internal and outlet stream flows and enthalpy values,

203 corresponding to the reference inlet power condition. Then, off-design calculation of the same system performance under different

204 electric power inputs can be performed, by interrogating a specific SOEC sub-model (MATLAB[TM] sub-routine); the SOEC sub-

9

205   model is based on external experimental data for a reference SOEC stack (see **Fig. 4**). The used experimental data derive from an

206   experimental study [23], in which a co-electrolyzer of SOEC technology has been tested in a limited set of operating

207   conditions. The empirical SOEC sub-model calculation provides, as output, data on the SOEC off-design operations (mainly the

208   reaction products outlet temperature, T_{OUT}, and the processed mass flow, $\dot{m}_{SOEC}$) which affect the behaviour of the other P2G sub-

209   sections. Thus, these data are used as input by the P2G system overall thermodynamic model (in ASPEN Hysys^{TM}), to obtain all the

210   stream flows and enthalpy values in the off-design operating point. Finally, the values of the several quantities in the off-design

211   operating point are transferred to MATLAB^{TM} environment, where performance parameters are calculated.

212   The HRS is necessary in order to pre-heat the water stream at the inlet of the system, using heat available at different

213   downstream sections of the P2G system. In more detail, heat is recovered from the SOEC outlet cathode and anode streams

214   and from all the methanation reactors cooling sections. The HRS heat-exchangers arrangement in the heat recovery line has

215   been optimized in the Authors' previous work [19] evaluating the temperature levels of the available heat flows. In particular,

216   it has been decided to place the HRS in the more heat demanding water line. Despite this, in order to feed the SOEC with

217   reactants at its operating temperature, an external heat source has also been considered.

218   When in off-design conditions, the values of the temperatures and of the mass flows of the streams involved in the HRS differ

219   from the values in design condition, mainly due to the different SOEC input electric power and outlet temperature.

220   In order to simulate the off-design behaviour of the HRS, first of all, the (U·A) values (where U [W/m^{2}K] is the global heat

221   transfer coefficient and A [m^2] is the heat exchanger surface) of each heat exchanger of this section have been calculated in

222   design conditions (these values have been obtained through the simulation of the P2G model in ASPEN Hysys^{TM}). In **Table 2**

223   the (U·A) values of the HRS in design condition for the four analysed configurations are reported. When the SOEC and the

224   HTM work at the same temperature value of 600 °C (Ambient 2 and Pressurized 2), the heat exchanger (HE-6) used to

225   recovery the heat from the stream at the outlet of the SOEC (and then at the inlet of the HTM) is not necessary. In these two

226   configurations, the heat exchanger with the highest value of UA is HE-1 (2115 W/K for Ambient 2 and 6047 W/K for

227   Pressurized 2). On the other hand, when the SOEC and the HTM work at different temperatures (Ambient 1 and Pressurized

228   1), an additional heat exchanger is required (HE-6) and it is the one with the highest value of UA.

229   After having obtained the (U·A) values in design condition, they have been kept constant also in off-design conditions.

230   Regarding the methanation sections (HTM and LTM), the chemical reactors work at the temperature set-point (see **Table 1**) and the

231   chemical reactions are able to follow the change of the mass flow value in off-design conditions.

232   Finally, the compression and separation section (C & Sep) considers the electrical energy consumption variation of the compressors

233   due to the different processed mass flow of the produced SNG in off-design conditions.

234   In the following paragraph, the co-electrolyzer off-design sub-model will be described.

235 **Table 2**. UA values of the HRS heat exchangers for the four analysed configurations in design condition (values obtained
236 through the simulation of the P2G model in ASPEN Hysys^{TM}).

	UA [W/K]			
	Ambient 1	**Ambient 2**	**Pressurized 1**	**Pressurized 2**
HE-1	2124	2115	4075	6047
HE-2	623.9	539.2	713.1	657.5
HE-3	117.9	120	221.9	134.7
HE-4	209	164.1	757.8	240.1
HE-5	2775	589.2	773.1	725.8
HE-6	5100	-	17290	-

237

3.1 Co-electrolyzer semi-empirical sub-model

239 The developed calculation sub-model (**Fig. 5**) allows to evaluate the outlet temperature and the electrical efficiency of the
240 SOEC in off-design conditions starting from input parameters. The knowledge of these two output parameters is essential in
241 order to predict the behaviour of the whole P2G system in off-design conditions; indeed, the SOEC efficiency strongly affects
242 the P2G system efficiency due to the high electrical energy consumption of this sub-section, while the outlet temperature value
243 determines the operating point of the other sub-sections.

244 The model inputs can be divided into two main categories: experimental data and actual operating conditions. In particular, the
245 empirical model requires, as experimental data, a limited number of information derived from an existing SOEC stack, used as
246 reference; the reference experimental data are: i) a set of polarization curves (i.e. voltage-current density of the experimental
247 stack) at different operating conditions, ii) the stack surface (A_{SOEC}) and iii) the stack inlet mass flow ($\dot{m}_{SOEC}$). The used
248 experimental data (polarization curves and stack data) derive from an experimental study [23], where a SOEC co-electrolyzer
249 has been tested under different pressure and temperature conditions.

250 The actual operating temperature (T_{SOEC}) and pressure (p_{SOEC}) are additional input of the off-design model and they can be
251 different from the temperature and pressure tested in the experiments.

252 The process flow of this sub-model can be divided into three steps:

253 i) calculation of generalized polarization curves;

254 ii) design condition definition;

255 iii) off-design performance evaluation.
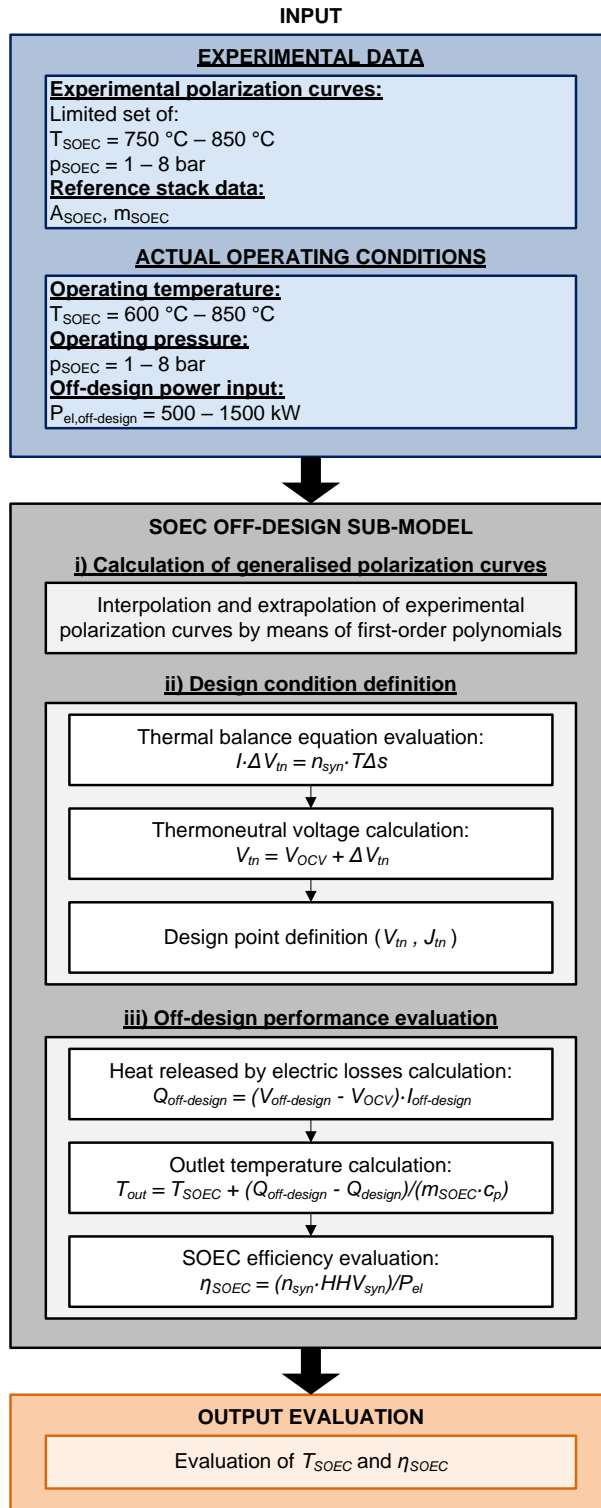
256 Each step of the sub-model will be described below.

11

EXPERIMENTAL DATA

Experimental polarization curves:
Limited set of:
T_{SOEC} = 750 °C – 850 °C
p_{SOEC} = 1 – 8 bar
Reference stack data:
A_{SOEC}, m_{SOEC}

ACTUAL OPERATING CONDITIONS

Operating temperature:
T_{SOEC} = 600 °C – 850 °C
Operating pressure:
p_{SOEC} = 1 – 8 bar
Off-design power input:
$P_{el,off-design}$ = 500 – 1500 kW

SOEC OFF-DESIGN SUB-MODEL

i) Calculation of generalised polarization curves

Interpolation and extrapolation of experimental polarization curves by means of first-order polynomials

ii) Design condition definition

Thermal balance equation evaluation:
$I \cdot \Delta V_{tn} = n_{syn} \cdot T\Delta s$

Thermoneutral voltage calculation:
$V_{tn} = V_{OCV} + \Delta V_{tn}$

Design point definition (V_{tn} , J_{tn})

iii) Off-design performance evaluation

Heat released by electric losses calculation:
$Q_{off-design} = (V_{off-design} - V_{OCV}) \cdot I_{off-design}$

Outlet temperature calculation:
$T_{out} = T_{SOEC} + (Q_{off-design} - Q_{design})/(m_{SOEC} \cdot c_p)$

SOEC efficiency evaluation:
$\eta_{SOEC} = (n_{syn} \cdot HHV_{syn})/P_{el}$

OUTPUT EVALUATION

Evaluation of T_{SOEC} and η_{SOEC}

257

258   **Fig. 5**. Flow chart of the SOEC off-design semi-empirical sub-model.

259

260   **i) Calculation of generalized polarization curves**

261   The first step of the sub-model consists in the calculation of generalized polarization curves, i.e. first-order polynomials that

262   describe the evolution of the cell voltage as a function of the current density. Starting from a limited set of experimental

263 polarization curves for the reference stack, the model is able to obtain the polarization curves of the SOEC under extended

264 operating conditions (inlet temperature and operating pressure) through the interpolation and extrapolation of the experimental

265 data with first-order polynomials (**Fig. 6a** and **Fig. 6b**); the slope of the polynomials has been obtained taking into account the

266 temperature and pressure variations.

267 The used experimental polarization curve points derive from an experimental study [23], in which a co-electrolyzer of SOEC

268 technology has been tested in a limited set of operating conditions (the investigated temperature range is 750-850 °C, while the

269 pressure range is 1-8 bar). Regarding the operating temperature, the experimental polarization curves have been extrapolated in

270 a wider range, between 600 °C and 850 °C, i.e. the extended operating range considered in this study (see **Fig. 6a**), typical for a

271 co-electrolyzer of SOEC technology [31]. Moreover, generalized polarization curves have been obtained also for different

272 pressure values, by interpolating the available experimental points (**Fig. 6b**).
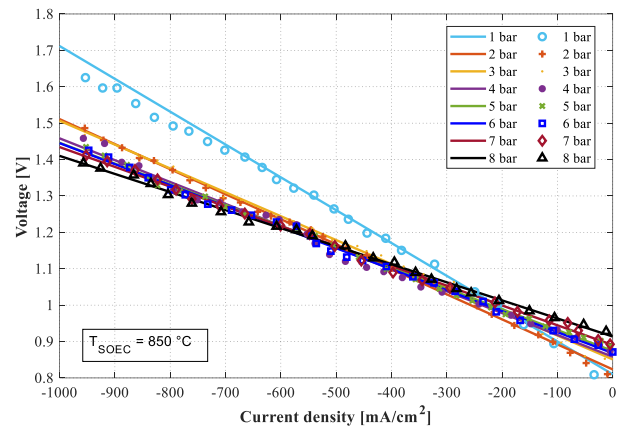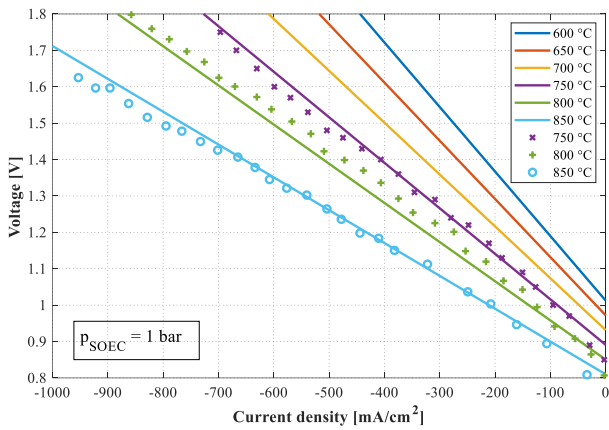
273

Fig. 6a. Generalized (extrapolated) polarization curves plotted for various operating temperature values, at p_{SOEC} = 1 bar (dots: experimental data points [23]; continuous lines: polynomial curves).

Fig. 6b. Generalized (interpolated) polarization curves plotted for various operating pressure values, at T_{SOEC} = 850 °C (dots: experimental data points [23]; continuous lines: polynomial curves).

274

275 **ii) Design condition definition**

276 The SOEC design operating point – i.e. the cell voltage and current density in design condition - has been identified on the

277 polarization curve for the actual operating conditions, by referring to the generalised experimental polarization curves.

278 In particular, in this study, the SOEC design point has been assumed coinciding with the "thermoneutral" condition, where the

279 thermoneutral voltage V_{tn} is defined as the potential at which the cell is thermally stable with respect to its equilibrium state at

280 V_{OCV} (Open Circuit Voltage) [32]. In thermoneutral condition, the heat released by the electric losses in the cell is equal to the

281 energy required by the co-electrolysis reactions. This operating condition is desirable for SOEC technology, in order to avoid

282 any additional device to provide heat or to extract it from the stack and this condition leads to have the same temperature value

283 for the inlet reactants and the outlet products.

284 In off-design conditions instead, the heat released by the electric losses in the cell differs from the energy required by co-

285 electrolysis reactions; in general, the electric energy demand due to the co-electrolysis reactions can be expressed as the

286 variation of the Gibbs free energy Δg:

287 $\Delta g = \Delta h - T \cdot \Delta s$ (5)

288 where, Δh [kJ/kmol] is the enthalpy variation of the co-electrolysis reactions, T [K] is the SOEC operating temperature equal

289 to the reactants inlet temperature and Δs [kJ/kmolK] is the entropy variation of the reactions; it must be highlighted that the

290 enthalpy variation and the entropy variation are influenced by the operating temperature and pressure of the SOEC.

291 If $V_{cell} < V_{tn}$ (endothermic mode), the electric energy Δg is lower than the enthalpy variation Δh and then additional heat is

292 required to maintain the operating temperature.

293 If instead $V_{cell} > V_{tn}$, the cell operates in the exothermic mode and this corresponds to an increase in the cell temperature,

294 because the electric energy supply Δg exceeds the enthalpy variation.

295 Thus, in order to evaluate the thermoneutral voltage, the following thermal balance equation has to be solved:

296 $I \cdot \Delta V_{tn} = \dot{n}_{syn} \cdot T\Delta s$ (6)

297 where, I [A] is the electric current of the SOEC $(I=J \cdot A_{SOEC})$, ΔV_{tn} [V] is the voltage related to the losses in thermoneutral

298 condition and $\dot{n}_{syn}$ [kmol/s] is the molar flow of produced syngas. According to the Faraday's Law (7), $\dot{n}_{syn}$ in the

299 electrochemical reactions can be expressed as:

300 $\dot{n}_{syn} = \frac{I}{ZF}$ (7)

301 where, Z is the valency number of ions of the substance and F [C/kmol] is the Faraday constant.

302 Then, eq. (6) can be reformulated as:

303 $\Delta V_{tn} = \frac{T\Delta s}{ZF}$ (8)

304 Finally, V_{tn} can be calculated by eq. (9):

305 $V_{tn} = V_{OCV} + \Delta V_{tn}$ (9)

306 Using the calculated V_{tn} value at given temperature and pressure, the corresponding design current density can be obtained

307 directly from the generalized polarization curve.

308

309

14

310 **iii) Off-design performance evaluation**

311 Once the design (thermoneutral) point is identified on the polarization curve, it is possible to identify the off-design point, i.e.

312 when the input electric power value ($P_{el,off-design}$ [W]) and the related current ($I_{off-design}$ [A]) and voltage ($V_{off-design}$ [V])

313 values differ from the design values; then, the new SOEC performance and in particular the updated SOEC outlet temperature

314 (T_{out} [K]) can be calculated in off-design operations. This temperature value coincides with the value of the inlet temperature

315 (T_{SOEC} [K]) only in design conditions. The off-design T_{out} estimation can be performed using the heat released by electric

316 losses in off-design conditions ($\dot{Q}_{off-design}$ [W]) expressed according to eq. (10):

317 $$\dot{Q}_{off-design} = \left(V_{off-design} - V_{OCV}\right) \cdot I_{off-design} \tag{10}$$

318 In this equation, in order to quantify the heat released by electric losses, the heat flux has been expressed as the product of the

319 electric current in off-design conditions and the difference between the voltage and the open circuit voltage (i.e. the voltage

320 given by the electric current flow in the circuit). Combining this equation with the expression of the heat released by electric

321 losses in thermoneutral condition ($\dot{Q}_{design}$ [W]), the outlet temperature in off-design conditions can be estimated as:

322 $$T_{out} = T_{SOEC} + \frac{\dot{Q}_{off-design} - \dot{Q}_{design}}{\dot{m}_{SOEC} \cdot c_p} \tag{11}$$

323 where $\dot{m}_{SOEC}$ is the actual SOEC inlet reactants mass flow [kg/s] and c_p [J/kgK] is the related specific heat.

324 Finally, the SOEC electrical efficiency [22] can be calculated according to:

325 $$\eta_{SOEC} = \frac{\dot{n}_{syn} \cdot HHV_{syn}}{P_{el}} \tag{12}$$

326 where, HHV_{syn} [kJ/kmol] is the higher heating value of the produced syngas and P_{el} [kW] is the electrical power input of the

327 SOEC related to the electrical current consumption of the cell ($P_{el}=V \cdot I$). According to (7), the SOEC efficiency is proportional

328 to a constant factor per applied voltage:

329 $$\eta_{SOEC} = \frac{HHV_{syn}}{ZF} \cdot \frac{1}{V} \propto \frac{constant}{V} \tag{13}$$

330 Then, the SOEC efficiency in off-design conditions can be calculated through the evaluation of the off-design voltage value.

331

332 **4. Analysis of the system coupled with renewables**

333 With the aim to evaluate the P2G system performance in off-design conditions, the coupling with a wind generator has been

334 considered. In this study, only a specific type of renewable generator (wind) has been evaluated, even if other renewable

335 sources can be exploited for this application; although a photovoltaic module, for example, presents an electricity production

336 profile quite different with respect to the wind, the proposed methodology and model are general and can be applied also to

337 other electrical energy sources.

15

338   The SOEC design electric power size for each P2G configuration has been set at 1 MW and, in the calculation of the overall

339   input power, also the compression and auxiliaries' consumption has been taken into account. The P2G off-design operating

340   range has been assumed between – 50 % and + 50 % of the design inlet power.

341   Regarding the coupled wind source, a year of production has been analyzed, taking into account the annual wind generation

342   duration curve data (see **Fig. 7**), referring to the Italian wind production (TERNA [33], [34]) available with a 5 min time step.

343   The wind annual production has a peak value equal to 1700 kW, while the mean annual wind power is equal to 750 kW,

344   corresponding to a nameplate power equal to 3 MW and 2200 equivalent hours of operation per year.

345   As already mentioned, the carried-out analysis is of quasi-static type. As a consequence, since the proposed model does not

346   consider process dynamics, the considered system has a time-dependent response, but the inertia effects have been neglected.

347   However, the process dynamics (accumulation of mass and energy in the several components of the plant) can play an

348   important role in the estimation of the system performance and this aspect will be considered in future studies.

349   The analysis has been carried out with a dedicated code, developed in MATLAB™ and integrated in the ASPEN Hysys™

350   environment. This code allows to evaluate the annual operating time of the P2G system, the surplus of electric energy not used

351   by the system – and then introduced into the electric grid or eventually wasted – and the values of the performance parameters.

352   In more detail, the code analyzes each time step of the year:

353   -   if, in the given time step, the electric power produced by the wind plant is lower than the lower operating limit of the P2G

354   system, then all the electric energy is introduced into the electric grid;

355   -   if, in the given time step, the electric power produced by the wind plant is within the operating range of the P2G plant, then

356   all the electric energy is employed within the process;

357   -   if, in the given time step, the electric power produced by the wind plant is greater than the upper operating limit of the P2G

358   system, then the difference between the wind production and the maximum electric load of the P2G system is introduced
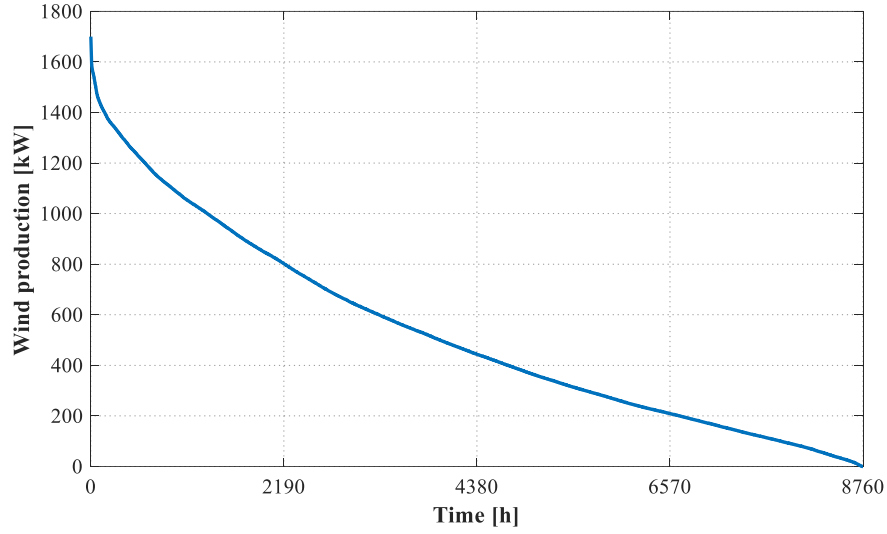
359   into the electric grid.

Fig. 7. The considered annual wind power production monotonic duration curve.

5. Preliminary economic analysis

In order to evaluate the cost effectiveness of the P2G technology, a preliminary economic analysis has been performed. The aim of this analysis is the estimation of the maximum investment cost of the P2G plant in order to have a competitive technology. In more detail, the economic feasibility of the whole project is evaluated through a cash flow analysis, based on the Net Present Value (NPV) defined as:

$$NPV = -I_0 + \sum_{i=1}^{t} \frac{CF_i}{(1+r)^i} \tag{14}$$

where, I_0 [€] represents the total initial investment (P2G system), r is the discount rate (assumed equal to 7 %), CF_i [€] is the net cash inflow at the i-th year and t [year] is the useful time horizon. The cash inflow for the general year i can be calculated as it follows:

$$CF_i = R_{SNG} - C_{O\&M} \tag{15}$$

where, R_{SNG} [€] is the revenue due to the SNG sell and $C_{O\&M}$ [€] is the operation and maintenance cost of the P2G plant. It should be highlighted that the electric power cost has not been taken into account due to the renewable generation. The $C_{O\&M}$ of the P2G plant has been assumed equal to 45 €/h according to [20]; the operation and maintenance cost has been related to the P2G operating time. In this economic analysis, a time horizon equal to 10 years has been assumed.

The aim of this analysis is to find the I_0 in order to have a return on the investment in the considered time horizon, varying the SNG cost. As a consequence, the economic problem can be expressed as:

$$NPV = 0 \ , I_0 = \sum_{i=1}^{n} \frac{CF_i}{(1+r)^i} \tag{16}$$

17

380 In the framework of a parametric analysis, the cost of the SNG has been varied from 0 to 100 €/MWh in order to evaluate the

381 P2G investment cost behaviour. It must be highlighted that in the SNG sell, only the methane content has been taken into

382 account.

383 In addition, in order to consider in the analysis a form of economic incentive for this emerging technology, a financial bonus in

384 the SNG sell has been considered. In more detail, an economic incentive equal to 32 €/MWh has been assumed, according to

385 the Italian legislation for biomethane injection into the natural gas grid [35].

386 In this economic analysis, the generated electricity that is introduced into the electric grid has not been accounted within the

387 cash flows. However, in order to evaluate the P2G process as an energy storage system, this quantity has been calculated

388 through the proposed model; indeed, with the aim to reduce over-generation (when the power production from renewables

389 exceeds the demand), the electric energy discharged to the grid can be a critical parameter to assess the performance of an

390 energy storage system. In addition, since the generated electricity introduced into the grid can be a marginal value of the

391 natural gas price, it will be analyzed in future studies.

392
393 **6. Results and discussion**

394 In this section, the results of the carried-out analysis are shown. In more detail, at first the results of the SOEC and of the HRS

395 sub-models are presented and, then, the results of the comparative analysis among the several P2G system configurations are

396 discussed. Finally, the results of the preliminary economic analysis are reported.

397

398 **6.1 Co-electrolyzer off-design performance**

399 In this section, the SOEC off-design non-dimensional curves, which represent the component behavior depending on the

400 operational load, are shown. In particular, in **Fig. 8a**, the normalized polarization curves (evolution of the cell voltage as a

401 function of the cell current density) for several operating temperatures are shown. All of these quantities are expressed in a

402 dimensionless form with respect to the design condition. The results show that, with the increase in the temperature, a lower

403 voltage is required for current densities lower than the design point – corresponding to the point (1;1) in the graph – while for

404 greater current densities the situation is the opposite. Furthermore, the pressurized SOEC behavior has been evaluated (**Fig.**

405 **8b**), considering a pressure range between 1 bar and 8 bar (experimental SOEC operating range) with a step equal to 1 bar. The

406 pressurization of the SOEC appears to be penalized due to the higher voltage requested for current densities lower than the

407 design point current density; for current densities higher than the design point current density, the situation is the opposite.
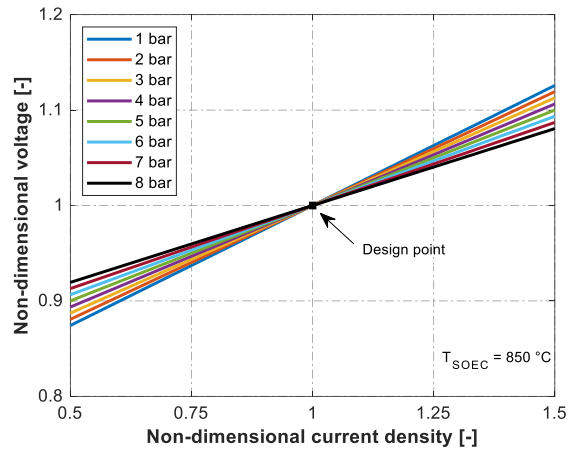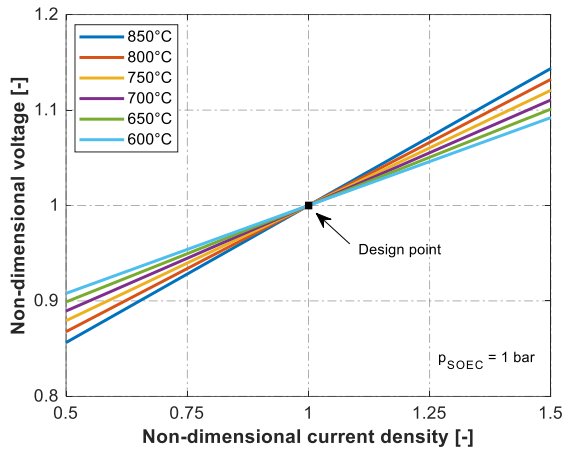
408

Fig. 8a. Effect of T$_{SOEC}$ on the normalised polarization curve for p$_{SOEC}$= 1 bar.

Fig. 8b. Effect of p$_{SOEC}$ on the normalised polarization curve for T$_{SOEC}$= 850 °C.

409

410 In **Fig. 9a**, the outlet temperature of the SOEC as a function of the electric load for several temperatures is presented. As it can

411 be noted, the outlet temperature varies from a minimum of about -15 % (for an electric load equal to 50 % of the design point)

412 to a maximum of about +13 % (for an electric load equal to 150 % of the design point), considering an operating temperature

413 of 850 °C. For lower operating temperatures the slope of the curve is lower. Indeed, for electrical loads lower than the design

414 point, the value of the voltage at set current density is higher for lower operating temperatures (see **Fig. 8a**) and, then, the

415 outlet temperature is higher, according to (10)-(11); for electrical loads higher than the design point, the situation is the

416 opposite: this leads to a slope of the curve lesser degree.

417 In **Fig. 9b**, the effect of the operating pressure on the outlet temperature of the SOEC as a function of the electric load is

418 shown. The outlet temperature varies from a minimum of about -11 % (for an electric load equal to 50 % of the design point)

419 to a maximum of about +10 % (for an electric load equal to 150 % of the design point), considering an operating pressure of 8

420 bar. In this case, for lower operating pressures the slope of the curve is higher. This behaviour can be explained through the

421 evaluation of the voltage (see **Fig. 8b**) for the several operating pressures, according to (10)-(11).
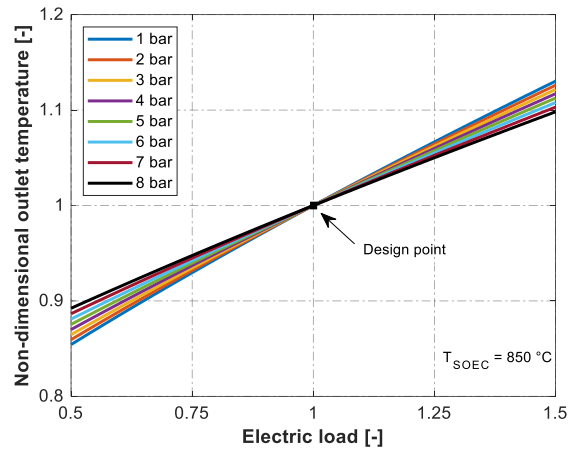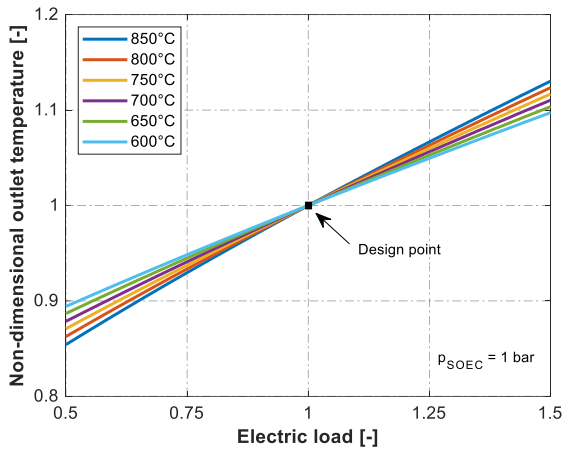
19

Fig. 9a. Normalised outlet temperature as a function of the electric load for several operating temperatures (p= 1 bar).

Fig. 9b. Normalised outlet temperature as a function of the electric load for several operating pressures (T= 850 °C).

422

423   The SOEC efficiency gain is shown as a function of the electrical load for several temperatures in **Fig. 10a.** In this figure, the

424   design point is represented by the point (0;1), with a null efficiency gain in correspondence of the design electric load. The

425   efficiency gain varies from a maximum of about + 14% (for an electric load equal to 50 % of the design point) to a minimum

426   of about -10 % (for an electric load equal to 150 % of the design point) for an operating temperature of 850 °C. Even in this

427   case, for lower operating temperatures the slope of the curve is lower.

428   The SOEC efficiency gain is presented as a function of the electrical load for several pressures in **Fig. 10b**. The efficiency gain

429   varies from a maximum of about +10 % (for an electric load equal to 50 % of the design point) to a minimum of about -7 %

430   (for an electric load equal to 150 % of the design point) for an operating pressure of 1 bar. For lower operating pressures the
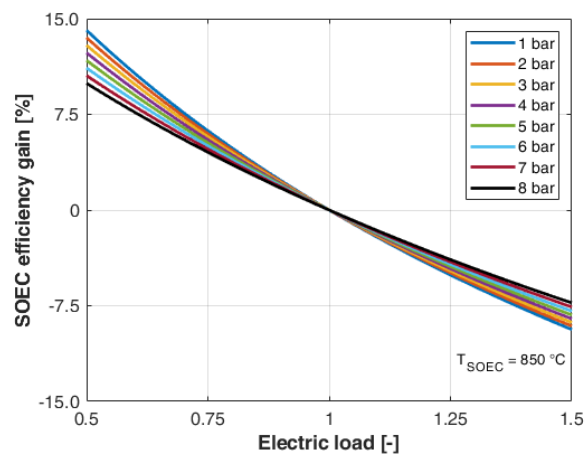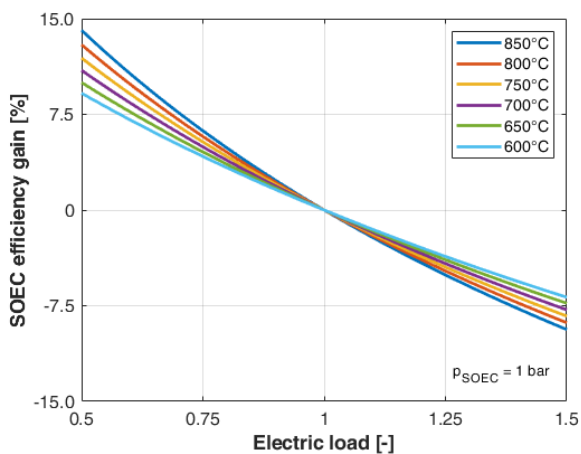
431   slope of the curve is higher.

Fig. 10a. SOEC efficiency gain as a function of the electric load for several operating temperatures (p= 1 bar).

Fig. 10b. SOEC efficiency gain as a function of the electric load for several operating pressures (T= 850 °C).

20

6.2 Heat recovery section off-design performance

In this section, the off-design performance of the HRS are shown. In particular, the HRS heat exchanged in design and off-design conditions for the four analyzed configurations is presented in **Fig. 11**. In all the considered configurations, the heat exchanger with the highest value of heat exchanged is HE-1, with a value between 105 kW and 109 kW in design condition. This situation is also confirmed in off-design conditions: HE-1 shows a value of the exchanged thermal power higher than 150 kW for all the analyzed configurations at 150 % of the load and a value of about 50 kW at 50 % of the load. Comparing configurations with the same temperature setting, the results are similar: indeed, for Ambient 1 (**Fig. 11a**) and Pressurized 1 (**Fig. 11c**), the thermal power exchanged in the whole HRS in design condition is equal to about 295 kW for both the configurations; Ambient 2 (**Fig. 11b**) shows a value of the thermal power exchanged in design condition slightly higher with respect to the configuration Pressurized 2 (**Fig. 11d**), respectively 242 kW and 233 kW.
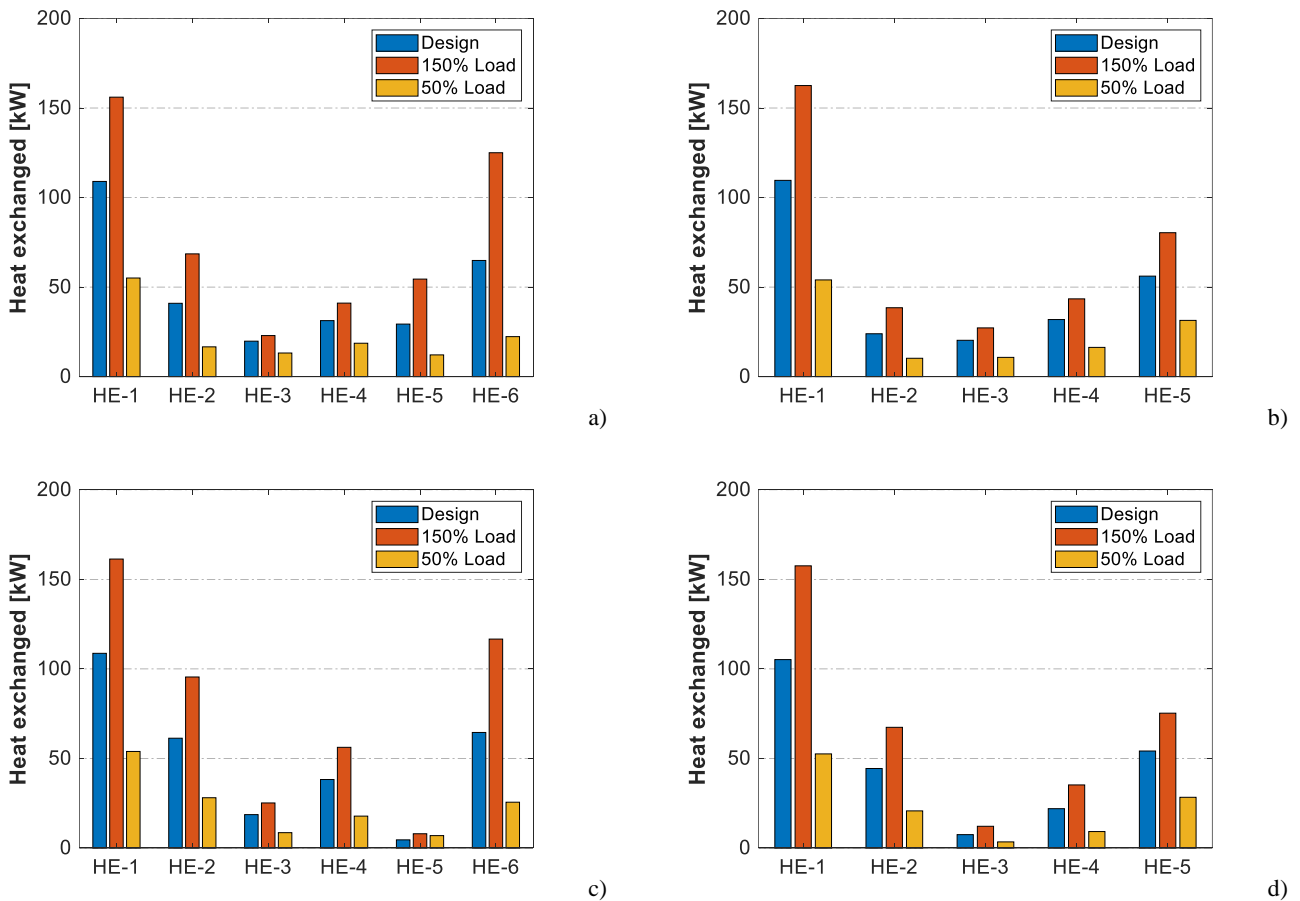

Fig. 11. HRS heat exchanged for the four analysed configurations in design and off-design conditions: a) Ambient 1; b) Ambient 2; c) Pressurized 1; d) Pressurized 2.

6.3 Power-to-Gas system performance

In **Table 3**, the results of the comparative analysis among the several considered variants are shown. The system Ambient 2 shows the highest number of operating hours, equal to 3896 h/year, due to the lowest electrical consumption with respect to the other variants. Indeed, while the SOEC input power is the same for all the variants, the overall electrical consumption is different and, in particular, higher for the pressurized systems. The operating time of the system Ambient 2 corresponds to about 45 % of the whole length of the year. Due to the lower operating time, the pressurized systems (Pressurized 1 and Pressurized 2) present a higher amount of electric energy introduced into the electric grid (1231 MWh/year for Pressurized 1 and 1224 MWh/year for Pressurized 2), and a lower energy utilization factor, equal to about 74 % for both the systems; on the contrary, the systems at ambient pressure (Ambient 1 and Ambient 2) show an energy utilization factor equal to about 75 %.

Regarding the SNG production, the systems at ambient pressure show higher values (216 ton/year for Ambient 2) with respect to the pressurized systems (188 ton/year for Pressurized 2). As a consequence, also the methane production follows the results of the SNG production; indeed, even if the SNG quality is higher for the pressurized systems, the systems at ambient pressure show a higher operating time and then a higher SNG production, that leads to a slightly higher methane production (184 ton/year for Ambient 2).

In order to evaluate the efficiency of the P2G variants throughout the year, the utilization efficiency (η_U) has been defined:

$$\eta_U = \frac{\sum_i \dot{m}_{SNG,i} \cdot LHV_{SNG,i}}{E_{WIND}} \tag{17}$$

where, $\dot{m}_{SNG,i}$ [kg/s] is the mass flow of produced SNG at the i-th instant of the year, $LHV_{SNG,i}$ [kJ/kg] is the lower heating value of the produced SNG at the i-th instant of the year and E_{WIND} [kWh] is the wind energy available in the whole year.

From the point of view of this efficiency, Ambient 2 shows better performance with respect to the other variants: indeed, for Ambient 2 the utilization efficiency is equal to 59 %.

In order to take into account also the thermal energy consumption, the overall first law efficiency has been introduced:

$$\eta_{I,TOT} = \frac{\sum_i \dot{m}_{SNG,i} \cdot LHV_{SNG,i}}{\sum_i P_{in,i} + \sum_i \dot{Q}_{in,i}} \tag{18}$$

where, $P_{in,i}$ [kW] is the P2G system inlet electric power at the i-th instant of the year and $\dot{Q}_{in,i}$ [kW] is the total amount of input heat required by the P2G system at the i-th instant of the year.

The system Ambient 1 shows better performance here too, with a value of about 75 %, even if the thermal consumption is higher for this system, with a value of about 175 MWh/year. This result can be explained through the evaluation of the SNG production, which results higher for this system.

473 **Table 3**. Annual results of the comparative analysis among the several P2G variants.

Parameter	Ambient 1	Ambient 2	Pressurized 1	Pressurized 2
P2G operating time [h/year]	3895	3896	3784	3797
Utilization factor [%]	44.4	44.5	43.2	43.3
Wind energy available [MWh/year]	4644	4644	4644	4644
Energy to the grid [MWh/year]	1175	1174	1231	1224
Energy utilization factor [%]	74.7	74.7	73.5	73.6
SNG production [ton/year]	215	216	189	188
CH_4 production [ton/year]	183	184	181	183
Total thermal energy externally requested [MWh/year]	160	175	117	154
Utilization efficiency [%]	58.3	59.0	55.1	55.3
Overall first law efficiency [%]	74.6	75.1	72.5	71.9

474

475 In order to analyse the off-design performance of the studied variants, the instantaneous values of the key calculated quantities

476 are presented in **Fig. 12-14**. In **Fig. 12**, the instantaneous SNG production throughout the year is shown. The system Ambient 2

477 presents a production slightly higher than the system Ambient 1 in the times of the year with the highest wind power

478 production (with a peak of about 0.028 kg/s), while when the wind production decreases the system Ambient 1 shows better

479 performance from this point of view. The pressurized systems present nearly the same SNG production, lower with respect to

480 the systems at ambient pressure. In **Fig. 13**, the instantaneous CH_4 production is shown. For all variants, the methane

481 production is about the same, with the system Pressurized 2 showing a slightly higher production, due to the higher quality of

482 the produced SNG. In **Fig. 14**, the instantaneous first law efficiency values are shown as a function of the wind production.

483 The trend of the first law efficiency highlights that the lower is the electric load, the higher is the efficiency due to the trend of

484 the SOEC efficiency (**Fig. 10a** and **Fig. 10b**). In particular, the system Ambient 1 shows a peak of about 0.82.
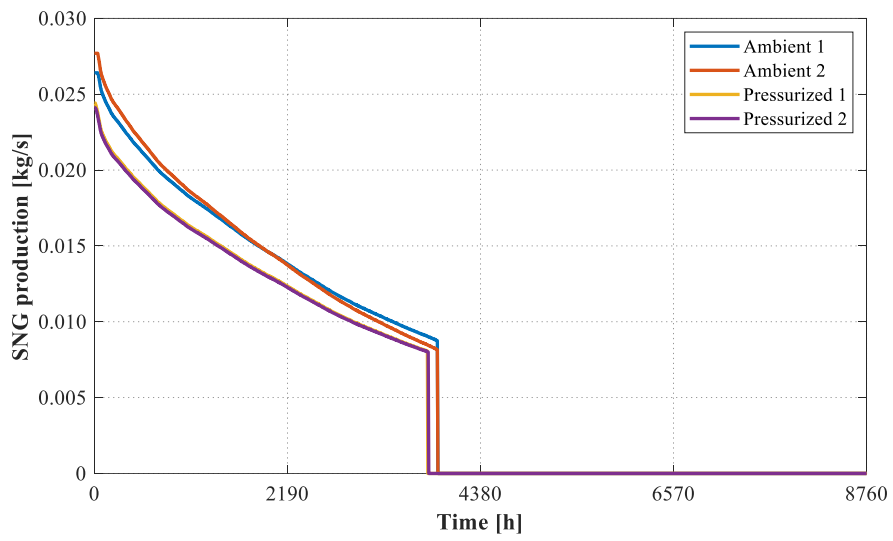
485

Fig. 12. The instantaneous SNG production during the year.
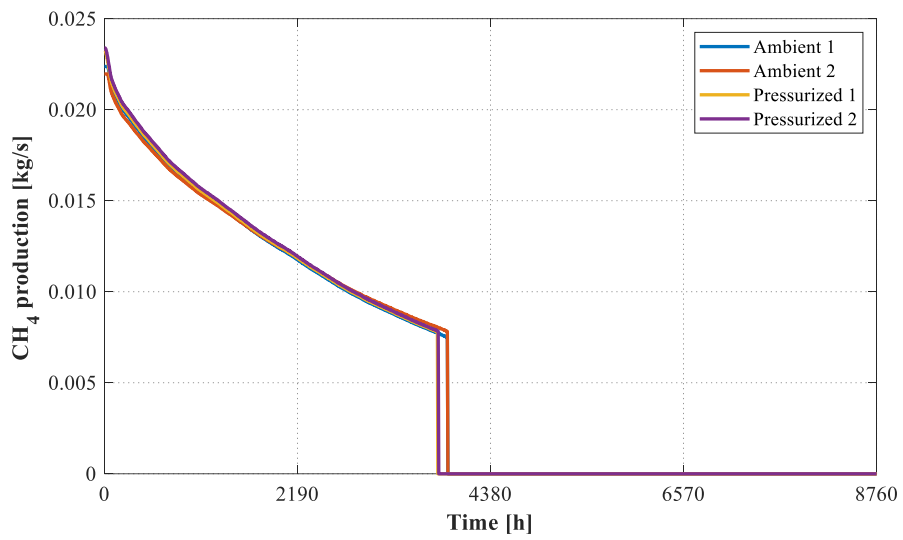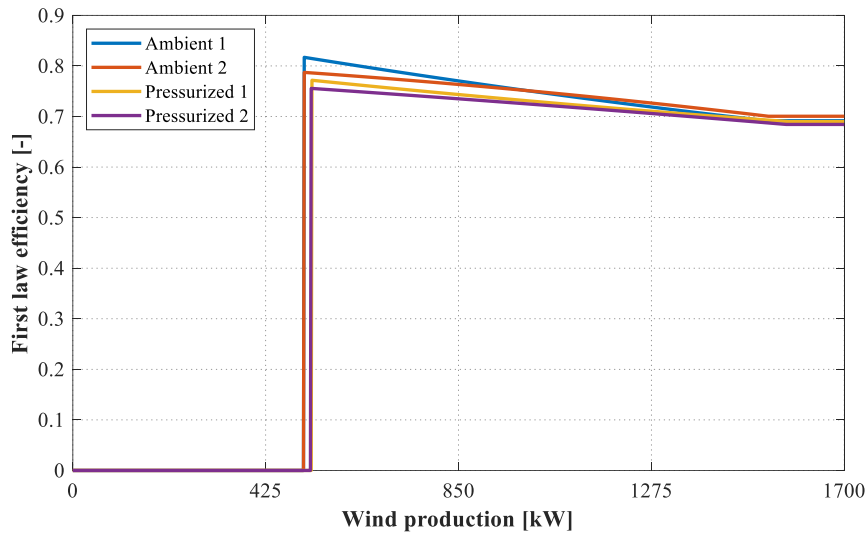
487

488

Fig. 13. The instantaneous CH_4 production during the year.

24

Fig. 14. The instantaneous first law efficiency as a function of the wind production.

6.4 Economic analysis

In this section, the results of the economic analysis are shown. In particular, in **Fig. 15** the investment cost per unit of P2G plant size as a function of the SNG cost is presented. The difference in the trend among the configurations is almost negligible, resulting in overlapping lines; thus, only configuration Ambient 2 has been considered in this section, since it leads to a higher methane production and a higher number of operating hours. The natural gas market price range is highlighted: lower bound corresponds to 2019 average NG price for industrial uses in Euro area (28.395 €/MWh); upper bound represents the 2019 average NG price for household consumers in Euro area (63.226 €/MWh). Both values refer to Eurostat [36]; NG prices for industrial uses are defined as follows: average national price without taxes applicable for the first semester of each year for medium size industrial consumers (annual consumption between 10000 GJ and 100000 GJ); on the other hand, NG prices for household consumers are defined as follows: average national price including taxes and levies applicable for the first semester of each year for medium size household consumers (annual consumption between 20 GJ and 200 GJ). With a SNG cost comprised in the NG market price range, configuration Ambient 2 has no return in the investment in the considered time horizon (10 years). Starting from a SNG cost of about 70 €/MWh, the P2G investment cost became positive coming up to a value of about 1500 €/MW for a SNG cost of 100 €/MWh. On the other hand, if the SNG sell is incentivised, there's a range of SNG cost (comprised between about 40 €/MWh and the household NG cost) in order to be competitive in the NG market.

In summary, the competitiveness of the studied technology (methanation coupled with high temperature co-electrolysis) is strongly dependent on the investment cost of the plant. Governments' action still might play a role in order to incentivise the SNG sell. Moreover, an increase in the renewable energy sources within the electricity production mix of a specific area could

result in a great impact on the local energy system; this will imply a progressive cost reduction of the produced electric energy. Also the full development of the SOEC technology is desirable in order to improve the competitiveness of the analysed system. Indeed, as reported by Schmidt et al. [37], the cost uncertainty is one of the most remarkable barriers to invest in electrolysis technology. On the other hand, the P2G process exhibits characteristics that distinguish itself with respect to the other storage technologies and could make it competitive in the energy market: i) it shows a potentially limitless storage capacity, if the produced SNG is introduced into the NG network; ii) the produced energy in the form of SNG is transportable even at great distances; iii) it could exploit the already available NG infrastructures.
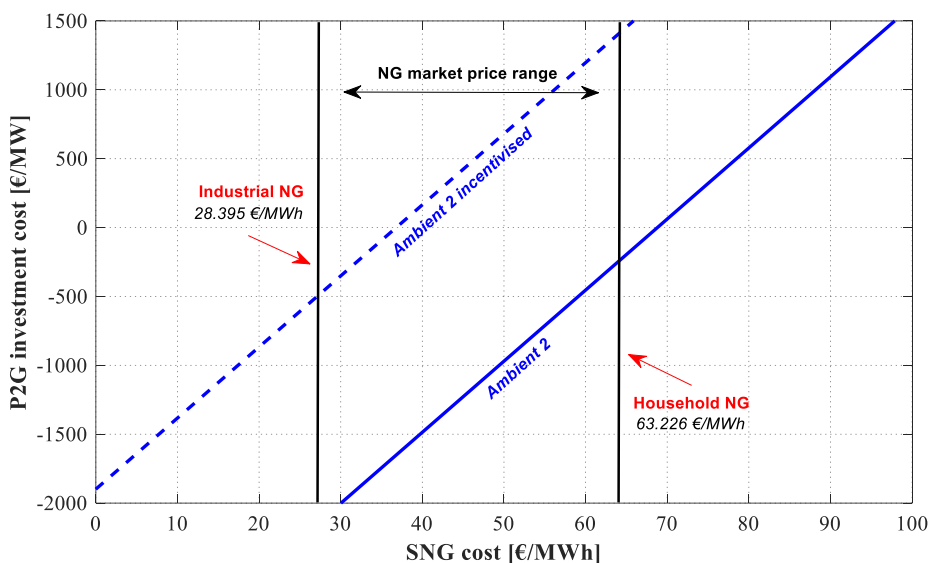
Fig. 15. Investment cost per unit of P2G plant size as a function of the SNG cost.

7. Conclusions

In this study, an innovative P2G system, based on a high temperature co-electrolyzer of SOEC technology coupled with an advanced experimental reactor, has been analysed in order to predict its off-design performance. In more detail, a numerical model has been developed for the P2G system and, in order to simulate the behaviour of the SOEC and of the HRS, specific calculation sub-models have been integrated in the whole system model. With the purpose of determining the performance of the considered P2G system in real operating conditions when coupled with renewables, a wind plant has been considered. In particular, during the analysis also the effect of the pressure on the system has been taken into account, evaluating four different configurations of the P2G process.

The results show that the most performant configuration is the one at ambient pressure, with the SOEC and the HTM operating at the same temperature (600 °C); indeed, this configuration presents higher values of the considered performance parameters with respect to the other configurations (a methane production equal to 184 ton/year and an overall efficiency of about 75 %).

26

532 Finally, with the aim to assess the cost effectiveness of the P2G process, a preliminary economic analysis has been performed;

533 the results point out that, in order to have a competitive technology, an economic incentive in the synthetic natural gas sell

534 must be applied.

535 Process dynamics (accumulation of mass and energy in the several components of the plant) can play an important role in the

536 estimation of the system performance and, then, this aspect will be considered in future studies.

537

538 **Nomenclature**

539 A   Area [m^2]

540 c   Specific heat [J/kgK]

541 E   Energy [kWh]

542 F   Faraday constant – 96485000 C/kmol

543 g   Specific Gibbs free energy [kJ/kmol]

544 h   Specific enthalpy [kJ/kmol]

545 HHV   Higher heating value [kJ/kg]

546 I   Electric current [A]

547 LHV   Lower heating value [kJ/kg]

548 J   Current density [A/m^2]

549 $\dot{m}$ Mass flow [kg/s]

550 $\dot{n}$ Molar flow [kmol/s]

551 P   Power [kW]

552 Q   Thermal power [W]

553 r Discount rate

554 s   Specific entropy [kJ/kmolK]

555 t   Time horizon [year]

556 t Temperature [K]

557 U   Global heat transfer coefficient [W/m^2K]

558 V   Voltage [V]

559 Z   Valency number of ions

560 **Greek symbols**

561 Δ   Difference

562	η	Efficiency
563	**Subscripts and Superscripts**	
564	el	Electrical
565	in	Inlet
566	OCV	Open circuit voltage
567	out	Outlet
568	p	Pressure
569	syn	Syngas
570	tn	Thermoneutral
571	**Acronyms**	
572	C	Compression
573	CF	Net cash inflow
574	el	Electrical
575	HT	High temperature
576	HTM	High temperature methanation
577	i	i-th
578	LT	Low temperature
579	LTM	Low temperature methanation
580	NG	Natural gas
581	NP-RES	Non-programmable renewable energy sources
582	NPV	Net present value
583	O&M	Operation and maintenance
584	P2G	Power-to-Gas
585	PV	Photovoltaic
586	R	Revenue
587	RES	Renewable energy sources
588	Sep	Separation
589	SNG	Synthetic natural gas
590	SOEC	Solid oxide electrolyte cell
591	TOT	Total

592	U	Utilization
593	vol	Volumetric
594	I	First law

References

592   U   Utilization

593   vol   Volumetric

594   I   First law

[1] C. Gerbaulet, C. von Hirschhausen, C. Kemfert, C. Lorenz, and P.-Y. Oei, 'European electricity sector decarbonization under different levels of foresight', *Renewable Energy*, vol. 141, pp. 973–987, Oct. 2019, doi: 10.1016/j.renene.2019.02.099.

[2] M. Karimi, H. Mokhlis, K. Naidu, S. Uddin, and A. H. A. Bakar, 'Photovoltaic penetration issues and impacts in distribution network – A review', *Renewable and Sustainable Energy Reviews*, vol. 53, pp. 594–605, Jan. 2016, doi: 10.1016/j.rser.2015.08.042.

[3] M. A. Eltawil and Z. Zhao, 'Grid-connected photovoltaic power systems: Technical and potential problems—A review', *Renewable and Sustainable Energy Reviews*, vol. 14, no. 1, pp. 112–129, Jan. 2010, doi: 10.1016/j.rser.2009.07.015.

[4] C. Jung, D. Taubert, and D. Schindler, 'The temporal variability of global wind energy – Long-term trends and inter-annual variability', *Energy Conversion and Management*, vol. 188, pp. 462–472, May 2019, doi: 10.1016/j.enconman.2019.03.072.

[5] M. A. Ancona *et al.*, 'Renewable Energy Storage System Based on a Power-to-Gas Conversion Process', *Energy Procedia*, vol. 101, pp. 854–861, Nov. 2016, doi: 10.1016/j.egypro.2016.11.108.

[6] Z. Yang, C. Gao, and M. Zhao, 'Coordination of integrated natural gas and electrical systems in day-ahead scheduling considering a novel flexible energy-use mechanism', *Energy Conversion and Management*, vol. 196, pp. 117–126, Sep. 2019.

[7] F. Sayedin, A. Maroufmashat, S. Sattari, A. Elkamel, and M. Fowler, 'Optimization of Photovoltaic Electrolyzer Hybrid systems; taking into account the effect of climate conditions', *Energy Conversion and Management*, vol. 118, pp. 438–449, Jun. 2016.

[8] M. Kopp, D. Coleman, C. Stiller, K. Scheffer, J. Aichinger, and B. Scheppat, 'Energiepark Mainz: Technical and economic analysis of the worldwide largest Power-to-Gas plant with PEM electrolysis', *International Journal of Hydrogen Energy*, vol. 42, no. 19, pp. 13311–13320, May 2017, doi: 10.1016/j.ijhydene.2016.12.145.

[9] J. Kupecki *et al.*, 'Energy analysis of a 10 kW-class power-to-gas system based on a solid oxide electrolyzer (SOE)', *Energy Conversion and Management*, vol. 199, p. 111934, Nov. 2019, doi: 10.1016/j.enconman.2019.111934.

620   [10] F. Petipas, A. Brisse, and C. Bouallou, 'Model-based behaviour of a high temperature electrolyser system operated

621   at various loads', *Journal of Power Sources*, vol. 239, pp. 584–595, Oct. 2013, doi: 10.1016/j.jpowsour.2013.03.027.

622   [11] H. Khani and H. E. Z. Farag, 'Optimal Day-Ahead Scheduling of Power-to-Gas Energy Storage and Gas Load

623   Management in Wholesale Electricity and Gas Markets', *IEEE Transactions on Sustainable Energy*, vol. 9, no. 2, pp.

624   940–951, Apr. 2018, doi: 10.1109/TSTE.2017.2767064.

625   [12] M. Frank, R. Deja, R. Peters, L. Blum, and D. Stolten, 'Bypassing renewable variability with a reversible solid oxide cell

626   plant', *Applied Energy*, vol. 217, pp. 101–112, May 2018, doi: 10.1016/j.apenergy.2018.02.115.

627   [13] G. Gahleitner, 'Hydrogen from renewable electricity: An international review of power-to-gas pilot plants for stationary

628   applications', *International Journal of Hydrogen Energy*, vol. 38, no. 5, pp. 2039–2061, Feb. 2013, doi:

629   10.1016/j.ijhydene.2012.12.010.

630   [14] K. Motylinski, M. Wierzbicki, S. Jagielski, and J. Kupecki, 'Investigation of off-design characteristics of solid oxide

631   electrolyser (SOE) operated in endothermic conditions', *E3S Web Conf.*, vol. 137, p. 01029, 2019, doi:

632   10.1051/e3sconf/201913701029.

633   [15] J. Kupecki, 'Off-design analysis of a micro-CHP unit with solid oxide fuel cells fed by DME', *International Journal of*

634   *Hydrogen Energy*, vol. 40, no. 35, pp. 12009–12022, Sep. 2015, doi: 10.1016/j.ijhydene.2015.06.031.

635   [16] J. Kupecki, J. Milewski, A. Szczesniak, R. Bernat, and K. Motylinski, 'Dynamic numerical analysis of cross-, co-, and

636   counter-current flow configuration of a 1 kW-class solid oxide fuel cell stack', *International Journal of Hydrogen*

637   *Energy*, vol. 40, no. 45, pp. 15834–15844, Dec. 2015, doi: 10.1016/j.ijhydene.2015.07.008.

638   [17] F. Safari and I. Dincer, 'Assessment and optimization of an integrated wind power system for hydrogen and methane

639   production', *Energy Conversion and Management*, vol. 177, pp. 693–703, Dec. 2018.

640   [18] Y. Luo, Y. Shi, W. Li, and N. Cai, 'Synchronous enhancement of H_2O/CO_2 co-electrolysis and methanation for

641   efficient one-step power-to-methane', *Energy Conversion and Management*, vol. 165, pp. 127–136, Jun. 2018, doi:

642   10.1016/j.enconman.2018.03.028.

643   [19] M. A. Ancona *et al.*, 'Thermal integration of a high-temperature co-electrolyzer and experimental methanator for Power-

644   to-Gas energy storage system', *Energy Conversion and Management*, vol. 186, pp. 140–155, Apr. 2019, doi:

645   10.1016/j.enconman.2019.02.057.

646   [20] E. Giglio, A. Lanzini, M. Santarelli, and P. Leone, 'Synthetic natural gas via integrated high-temperature electrolysis

647   methanation: Part II—Economic analysis', *Journal of Energy Storage*, vol. 2, pp. 64–79, Aug. 2015, doi:

648   10.1016/j.est.2015.06.004.

649   [21] M. Lo Faro, S. C. Zignani, S. Trocino, V. Antonucci, and A. S. Aricò, 'New insights on the co-electrolysis of CO2 and

650   H2O through a solid oxide electrolyser operating at intermediate temperatures', *Electrochimica Acta*, vol. 296, pp. 458–

651   464, Feb. 2019, doi: 10.1016/j.electacta.2018.11.079.

652   [22] M. Gruber *et al.*, 'Power-to-Gas through thermal integration of high-temperature steam electrolysis and carbon dioxide

653   methanation - Experimental results', *Fuel Processing Technology*, vol. 181, pp. 61–74, Dec. 2018, doi:

654   10.1016/j.fuproc.2018.09.003.

655   [23] M. T. Mehran *et al.*, 'Production of syngas from H2O/CO2 by high-pressure coelectrolysis in tubular solid oxide cells',

656   *Applied Energy*, vol. 212, pp. 759–770, Feb. 2018, doi: 10.1016/j.apenergy.2017.12.078.

657   [24] S.-W. Kim *et al.*, 'Reactions and mass transport in high temperature co-electrolysis of steam/CO2 mixtures for syngas

658   production', *Journal of Power Sources*, vol. 280, pp. 630–639, Apr. 2015, doi: 10.1016/j.jpowsour.2015.01.083.

659   [25] J. H. Jensen, J. M. Poulsen, and N. U. Andersen, 'From coal to clean energy', *Nitrogen+Syngas*, vol. 310, pp. 34–38,

660   2011.

661   [26] 'Aspen HYSYSTM'. [Online]. Available: https://www.aspentech.com/.

662   [27] HELMET EU, 'HELMET EU project'. [Online]. Available: http://www.helmeth.eu/.

663   [28] M. Samavati, M. Santarelli, A. Martin, and V. Nemanova, 'Thermodynamic and economy analysis of solid oxide

664   electrolyser system for syngas production', *Energy*, vol. 122, pp. 37–49, Mar. 2017, doi: 10.1016/j.energy.2017.01.067.

665   [29] 'Snam Rete Gas - Italian National Natural Gas Utility'. [Online]. Available: https://www.snam.it/it/index.html.

666   [30] 'MATLAB'. [Online]. Available: https://www.mathworks.com/.

667   [31] M. A. Laguna-Bercero, 'Recent advances in high temperature electrolysis using solid oxide fuel cells: A review',

668   *Journal of Power Sources*, vol. 203, pp. 4–16, Apr. 2012, doi: 10.1016/j.jpowsour.2011.12.019.

669   [32] J. Aicart, 'Modélisation et validation expérimentale d'un co-électrolyseur de la vapeur d'eau et du dioxyde de carbone à

670   haute température', thesis, Grenoble, 2014.

671   [33] 'TERNA'. [Online]. Available: 18.   https://www.terna.it/it-it/sistemaelettrico/statisticheeprevisioni/datistatistici.aspx.

672   [34] M. A. Ancona *et al.*, 'Off-Design Performance Evaluation of a LNG Production Plant Coupled with Renewables', in

673   *Proceedings of ASME Turbo Expo 2019: Turbomachinery Technical Conference and Exposition*, Phoenix, Arizona,

674   USA, 2019, pp. 1–12.

675   [35] Ministero delle Infrastrutture e dei Trasporti, *Approvazione del glossario contenente l'elenco non esaustivo delle

676   principali opere edilizie realizzabili in regime di attività edilizia libera*. 2018.

677   [36] Eurostat, 'Gas prices by type of users', 2019. [Online]. Available: https://ec.europa.eu/eurostat/web/products-datasets/-

678   /ten00118.

679   [37]   O. Schmidt, A. Gambhir, I. Staffell, A. Hawkes, J. Nelson, and S. Few, 'Future cost and performance of water

680   electrolysis: An expert elicitation study', *International Journal of Hydrogen Energy*, vol. 42, no. 52, pp. 30470–30492,

681   Dec. 2017, doi: 10.1016/j.ijhydene.2017.10.045.

682